H_2O windows and CO_2 radiator fins: a clear-sky explanation for the peak in ECS

Jacob T. Seeley[1], Nadir Jeevanjee[2]

[1]Harvard University Center for the Environment
[2]Geophysical Fluid Dynamics Laboratory

Key Points:

- A simple 1-dimensional climate model exhibits a peak in equilibrium climate sensitivity (ECS) at a surface temperature of around 310 K
- This peak in ECS arises from a competition between decreasing emission from the H_2O "windows" and increasing emission from CO_2 "radiator fins".
- Moist-adiabatic warming in the upper troposphere is key for the efficacy of the CO_2 radiator fins, and hence for the ECS peak.

Corresponding author: Jacob T. Seeley, `jacob.t.seeley@gmail.com`

Abstract

Recent explorations of the state-dependence of Earth's equilibrium climate sensitivity (ECS) have revealed a pronounced *peak* in ECS at a surface temperature of approximately 310 K. This ECS peak has been observed in models spanning the model hierarchy, suggesting a robust physical source. Here we propose an explanation for this ECS peak using a novel spectrally-resolved decomposition of clear-sky longwave feedbacks. We show that the interplay between spectral feedbacks in H_2O- and CO_2-dominated portions of the longwave spectrum, along with moist-adiabatic amplification of upper-tropospheric warming, conspire to produce a minimum in the feedback parameter, and a corresponding peak in ECS, at a surface temperature of 310 K. Mechanism denial tests highlight three key ingredients for the ECS peak: 1) H_2O continuum absorption to quickly close spectral windows at high surface temperature; 2) moist-adiabatic tropospheric temperatures to enhance upper-tropospheric warming; and 3) energetically-consistent increases of CO_2 with surface temperature.

Plain Language Summary

Earth's equilibrium climate sensitivity (ECS) is roughly defined as the equilibrium change in surface temperature resulting from a doubling of CO_2. It is well-known that ECS can exhibit a considerable state-dependence, in that its value depends on both the baseline surface temperature and CO_2 concentration. Curiously, recent explorations of the state-dependence of ECS have revealed the presence of a pronounced peak in ECS at a surface temperature of approximately 310 K, with ECS then decreasing at higher surface temperatures and CO_2 concentrations. Here we propose an explanation for this peak in ECS that depends only on clear-sky longwave feedbacks. Our explanation attributes the peak in ECS to a minimum in the magnitude of the feedback parameter, which occurs as the system transitions between two different methods of re-equilibrating to an imposed energy imbalance. At low surface temperature and CO_2, Earth re-equilibrates to an imposed imbalance by changing the amount of radiation escaping to space through spectral windows where the opacity of H_2O is low. At high surface temperatures and CO_2 concentrations, these H_2O "windows" have closed, and Earth re-equilibrates primarily by changing the amount of radiation escaping to space in spectral intervals where CO_2 opacity dominates over H_2O opacity.

1 Introduction

Earth's equilibrium climate sensitivity (ECS) is arguably the most studied quantity in climate science, with a history going back over 100 years and intensive study continuing to the present day (Arrhenius, 1896; Knutti et al., 2017). Roughly defined as the equilibrium change in surface temperature resulting from a doubling of CO_2, ECS has mostly been studied in the anthropogenic context of a doubling of CO_2 relative to its preindustrial value. It is well-known, however, that ECS can exhibit a considerable *state-dependence*, in that its value depends on both the baseline surface temperature and CO_2 concentration. This has been seen in both global climate models as well as the paleoclimate record (Knutti & Rugenstein, 2015; Bloch-Johnson et al., 2015; Rohling et al., 2012, and references therein).

In modeling studies, this state-dependence often takes the form of an increase in ECS with increasing surface temperature and CO_2. Since ECS can be understood as the ratio

$$\mathrm{ECS} = \frac{F_{2\mathrm{x}}}{\lambda_{\mathrm{eff}}} \tag{1}$$

of the radiative forcing from doubling CO_2, $F_{2\mathrm{x}}$ (W/m^2), to an effective feedback parameter, λ_{eff} (W/m^2/K), the state-dependence of ECS can also be understood in these terms. In terms of forcing, it is understood that $F_{2\mathrm{x}}$ increases monotonically with surface temperature and CO_2, due to both increasing surface-atmosphere temperature contrast as well as increasing radiative efficacy of secondary CO_2 bands (Seeley et al., 2020; Jeevanjee et al., 2020; Zhong & Haigh, 2013). In terms of feedbacks, a decrease in λ_{eff} (which increases ECS) would be expected from an increase in the water-vapor feedback, and in particular the closing of the water vapor spectral "window" (e.g. Koll & Cronin, 2018). But, recent explorations of the state-dependence of ECS have revealed an even more curious phenomemon, namely the presence of a pronounced *peak* in ECS at a surface temperature of approximately 310 K, with ECS then decreasing at higher T_{s} and CO_2 concentrations (Romps, 2020; Wolf et al., 2018; Popp et al., 2016; Wolf & Toon, 2015; Russell et al., 2013; Leconte et al., 2013; Meraner et al., 2013).

This ECS peak has been observed in models spanning the model hierarchy, from single column models to comprehensive coupled GCMs. The proposed explanations for the peak are also diverse, ranging from longwave clear-sky feedbacks (Meraner et al., 2013) to various cloud feedbacks (Wolf et al., 2018; Wolf & Toon, 2015; Russell et al., 2013). While a diversity of feedbacks is likely involved, the ubiquity of the ECS peak suggests that a rather fundamental mechanism is at play, stemming from robust physics and not reliant on, say, uncertain cloud parameterizations. Forcing is not a candidate for the ECS peak either, as $F_{2\mathrm{x}}$ is monotonic in T_{s} and CO_2.

This state of affairs was highlighted in the recent work of Romps (2020), which studied cloud-resolving simulations of radiative-convective equilibrium with a closed surface energy budget. Using a novel equilibration technique which allowed for a near-continuous exploration of a large range of CO_2 concentrations, Romps (2020) found a dramatic and well-resolved ECS peak, again in the neighborhood of 310 K. This peak was again attributed to a peak in λ_{eff}, not $F_{2\mathrm{x}}$. Moreover, these simulations have small cloud fraction maxima (relative to GCMs) of roughly 10% or less, again pointing away from poorly constrained cloud feedbacks and towards something more fundamental.

These findings motivated us to search for an explanation for the ECS peak in terms of only clear-sky longwave feedbacks. Here, we propose such an explanation which relies only on the CO_2 and H_2O greenhouse effects, as well as the thermodynamics of moist adiabats, consistent with the analysis of Meraner et al. (2013). Our explanation rests on a novel *spectrally-resolved* feedback decomposition, rather than the traditional decomposition of clear-sky feedbacks (i.e. Planck, lapse rate, and water vapor). As we will show, the interplay between spectral feedbacks in H_2O- and CO_2-dominated portions of the longwave spectrum, along with moist-adiabatic amplification of temperature change in the upper troposphere, conspire to produce a pronounced minimum in λ_{eff} and a corresponding peak in ECS, at a surface temperature of approximately 310 K.

2 Methods

2.1 A very simple climate model

In this work, we study the ECS of a very simple 1-D "climate model" in the spirit of the earliest climate models that included a convective adjustment (Manabe et al., 1964). The thermal structure of the atmosphere is assumed to follow the pseudoadiabatic lapse rate in the troposphere, with an overlying isothermal stratosphere at the tropopause temperature T_{tp}. Relative humidity RH in the troposphere is assumed to be vertically-uniform, and the H_2O mass fraction in the stratosphere is set equal to its value at the tropopause. Our default values for T_{tp} and RH are 200 K and 75%, respectively, but we test the sensitivity of our results to plausible changes in these values. The surface pressure is fixed at 101325 Pa (therefore ignoring the increase in column mass from increasing CO_2 and H_2O at high T_{s}).

Since we only consider longwave radiative transfer in this work, our definition of an equilibrated climate state is based solely on the value of outgoing longwave radiation

(OLR) rather than the net (shortwave + longwave) flux at the top-of-atmosphere. Accordingly, our equilibration procedure is as follows: for each experimental configuration (i.e., each combination of T_{tp}, RH, and any other varied parameters), we first calculated the OLR for $T_{\mathrm{s}} = 300$ K with 280 ppm of CO_2. We call this value OLR_0. Next, for each other surface temperature under consideration, we adjusted the CO_2 amount until the OLR was equal to OLR_0 (to within a precision of 10^{-2} W/m^2). This yields pairs of values of T_{s} and C, where C is the equilibrated CO_2 concentration. We carry out this procedure for surface temperatures between 285 and 330 K at 1-K increments. With the resulting pairs of T_{s} and C, we can then construct, by interpolation, the functions $T_{\mathrm{s}}(C)$ and $C(T_{\mathrm{s}})$ (following Romps, 2020). The ECS, as a function of T_{s}, is then given by

$$\mathrm{ECS}(T_{\mathrm{s}}) = T_{\mathrm{s}}[2 \times C(T_{\mathrm{s}})] - T_{\mathrm{s}}. \tag{2}$$

Again, by defining equilibration in terms of OLR only, rather than net flux, these calculations assume the shortwave feedback is zero.

2.2 Radiative transfer modelling

The radiative transfer calculations are the most complex aspect of our simple climate model. We used the Reference Forward Model (RFM) (Dudhia, 2017), a contemporary line-by-line code, to compute spectrally-resolved OLR for the 1-D atmospheric soundings of our simple climate model. Our calculations cover the spectral range from 0–3000 cm^{-1} with a resolution of $\Delta\nu = 0.1$ cm^{-1}, and our vertical grid extends from the surface to a height of 60 km with a vertical grid spacing of $\Delta z = 200$ m. We calculated radiative fluxes via the two-stream approximation with first-moment Gaussian quadrature (Clough et al., 1992). Our spectroscopic data was drawn from the latest version of the HITRAN database (Gordon et al., 2017); we used HITRAN data for all available isotopes of CO_2 and H_2O, weighted by their relative abundances (as is HITRAN convention). The RFM calculates atmospheric layer opacities on the user-supplied spectral grid by summing the contributions from all local lines with a lineshape truncation of 25 cm^{-1}. The RFM models the sub-Lorentzian far wings of CO_2 lines with the so-called χ-factor approach (Cousin et al., 1985), and continuum absorption is modelled with version 3.2 of the MTCKD code (Mlawer et al., 2012).

3 Results

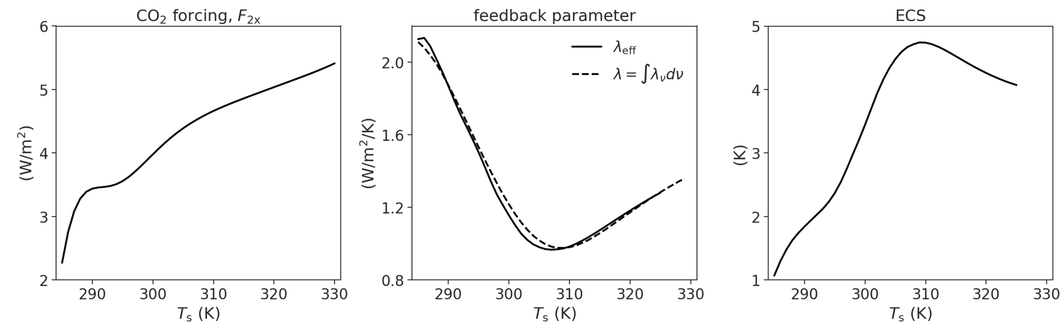

Figure 1. From the simple 1-D climate model, as a function of surface temperature T_{s}: (left) the radiative forcing from doubling CO_2 (eqn. 3); (center) the effective feedback parameter λ_{eff}, compared to the differential feedback parameter λ (eqn. 4); (right) the ECS (eqn. 2).

3.1 The peak in ECS

The rightmost panel of Figure 1 plots ECS as a function of T_s from our simple climate model in its default configuration (with $T_\mathrm{tp} = 200$ K and RH = 75%). We find a peak in ECS occurring at approximately the same surface temperature (slightly below 310 K) as was obtained by Romps (2020) in a cloud-resolving model, although our peak is not as sharp. The existence of this peak in ECS is robust to reasonable changes in tropospheric RH and tropopause temperature T_tp, but the temperature at which the peak occurs is delayed by decreasing the RH, and vice versa (Fig. S1).

As has been found in prior work, our peak in ECS is attributable to a minimum in λ_eff at nearly the same surface temperature (Fig. 1). We calculate λ_eff as F_2x/ECS (eqn. 1), where F_2x is calculated as

$$F_\mathrm{2x}(T_\mathrm{s}) = \mathrm{OLR}[T_\mathrm{s}, C(T_\mathrm{s})] - \mathrm{OLR}[T_\mathrm{s}, 2 \times C(T_\mathrm{s})]. \tag{3}$$

Note that the first panel of Figure 1 confirms that F_2x is not a candidate explanation for the peak in ECS, since it increases monotonically with surface temperature due to increasing surface-atmosphere temperature contrast and increasing radiative efficacy of secondary CO_2 bands (Seeley et al., 2020; Jeevanjee et al., 2020; Zhong & Haigh, 2013).

Therefore, to explain the ECS peak, we must explain why λ_eff has a minimum. To this end, it is helpful to note that the effective feedback λ_eff can be approximated by the differential feedback parameter, λ, which is obtained by incrementing the surface temperature by 1 K and taking a finite difference in OLR:

$$\lambda(T_\mathrm{s}) = \{\mathrm{OLR}[T_\mathrm{s}+1, 2 \times C(T_\mathrm{s})] - \mathrm{OLR}[T_\mathrm{s}, 2 \times C(T_\mathrm{s})]\}/(1\ \mathrm{K}). \tag{4}$$

The use of $2{\times}C$ in the definition of λ is justified by the fact that, in the context of ECS, we are interested in the feedback that operates *after* CO_2 has been doubled. Also, note that when we increment the surface temperature by 1 K, we use the moist-adiabatic sounding associated with that warmer surface temperature, which means that the conventional lapse rate and fixed-RH water vapor feedbacks are baked into the response. The middle panel of Figure 1 shows that $\lambda_\mathrm{eff} \simeq \lambda$, which validates the forcing-feedback framework in this context: a clean delineation between forcing and feedback, as is assumed by equation (1), requires that the forcing is not too sensitive to the climate change it induces. A close match between λ and λ_eff also requires that the state-dependence of feedbacks does not cause the assumption of a linear climate response to fail (e.g., Bloch-Johnson et al., 2015). Given this close match, we turn our attention to understanding λ.

3.2 Spectral feedback analysis

To better understand the minimum in λ, we conducted a spectral feedback analysis. Since OLR is a spectral integral over wavenumber, the differential feedback parameter can be obtained by integrating the *spectral* differential feedback parameter:

$$\lambda = \int \lambda_\nu \, \mathrm{d}\nu, \tag{5}$$

where λ_ν is given by the spectral version of equation (4):

$$\lambda_\nu(T_\mathrm{s}) = \{\mathrm{OLR}_\nu[T_\mathrm{s}+1, 2 \times C(T_\mathrm{s})] - \mathrm{OLR}_\nu[T_\mathrm{s}, 2 \times C(T_\mathrm{s})]\}/(1\ \mathrm{K}). \tag{6}$$

The top row of Figure 2 shows the spectrally-resolved differential feedbacks for $T_\mathrm{s} =$ 285 and 305 K. We focus on the wavenumber interval from 100–1500 cm^{-1}, which accounts for $> 85\%$ of the total feedback for all surface temperatures. Conceptually, λ_ν can be divided into three categories based on the total column optical depths of CO_2 and H_2O ($\tau_\mathrm{s}^{\mathrm{CO_2}}$ and $\tau_\mathrm{s}^{\mathrm{H_2O}}$; bottom row of Fig. 2). The first category includes spectral regions

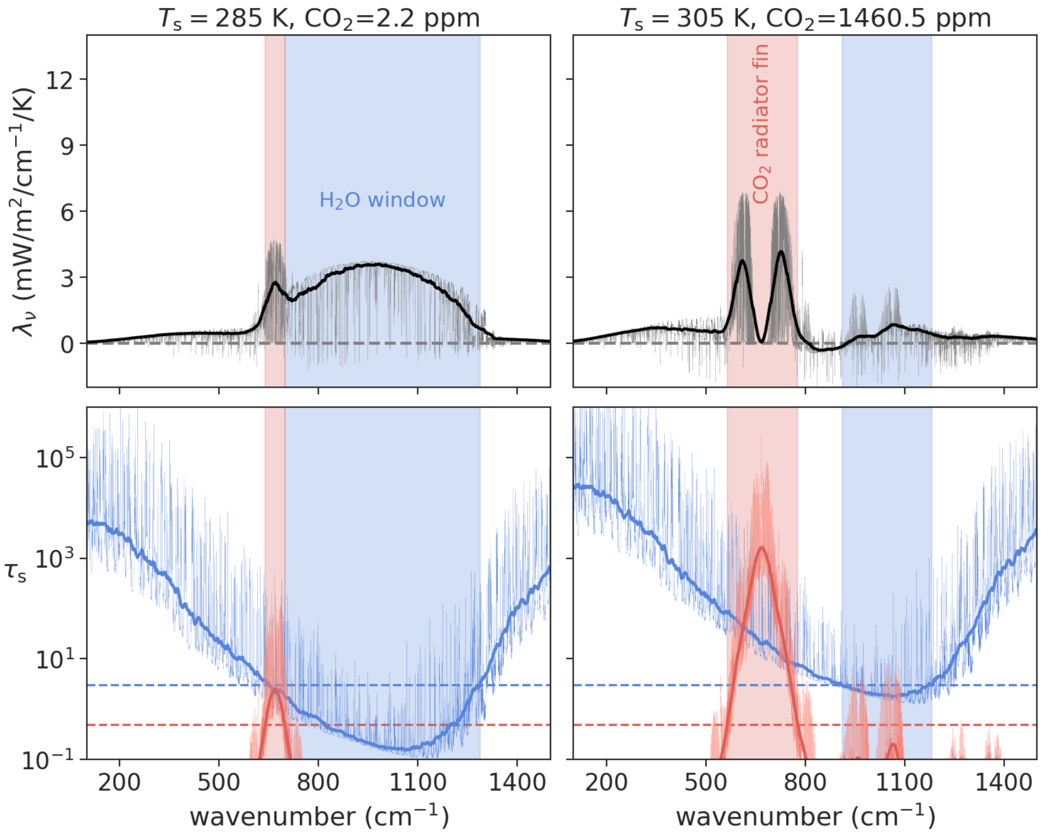

Figure 2. For $T_s = 285$ and 305 K: (top row) the spectral differential feedbacks λ_ν (eqn. 6); (bottom row) the surface optical depths of CO_2 and H_2O ($\tau_s^{CO_2}$ and $\tau_s^{H_2O}$, respectively). Note that the CO_2 concentrations specified at the top of the plot are twice the equilibrated concentration at each surface temperature, in accordance with equation (6). In all panels the thin lines show results at our default spectral resolution of $\Delta\nu = 0.1$ cm^{-1}, while the solid lines show smoothed data (i.e., a centered mean with window width 25 cm^{-1}; for the optical depths, the mean is take geometrically). The red shaded portion of the spectrum ("CO_2 radiator fin") has smoothed $\tau_s^{CO_2} > 0.5$ (dashed horizontal red line in bottom row). The blue shaded portion ("H_2O window") has smoothed $\tau_s^{H_2O} < 3$ (dashed horizontal blue line in bottom row) and smoothed $\tau_s^{CO_2} < 0.5$.

within which H_2O is optically thick but CO_2 has negligible opacity (we will make these definitions precise momentarily). These spectral regions exhibit a near-zero λ_ν due to the fact that H_2O optical depths are approximately invariant functions of temperature within the atmosphere (i.e., they are independent of surface temperature). We refer to this first category of wavenumbers as "Simpsonian", as the implication of T_s-invariant H_2O optical depths for OLR has been recognized since the pioneering work of G. Simpson (1928). In Figure 2, the Simpsonian spectral regions are those that have not been color-coded red or blue, corresponding to optically-thick portions of the pure rotational and vibrational-rotational bands of H_2O that are not overlapped by CO_2 absorption. The fact that $\lambda_\nu \simeq 0$ in the extensive Simpsonian spectral intervals explains why water vapor significantly reduces λ compared to a pure Planck response (Ingram, 2010; Koll & Cronin, 2018).

The second category of λ_ν includes spectral regions within which H_2O is *not* optically thick, and within which CO_2 also has negligible opacity (Fig. 2, blue shading). The importance of these spectral "windows" in allowing a warmer Earth to emit more radiation to space was also recognized quite early on by Simpson (G. C. Simpson, 1928). Indeed, at the cooler surface temperature of 285 K shown in Figure 2, λ_ν is non-zero primarily in the H_2O window, between approximately 700–1300 cm^{-1}, where the increase in upwelling radiation from the surface is relatively efficiently communicated out to space. However, as can be seen by comparing λ_ν for 285 and 305 K, as T_s increases and H_2O accumulates in the atmosphere, H_2O column opacity for a given absorption coefficient grows, and the H_2O window shrinks from the outside in. As was recently emphasized by Koll & Cronin (2018), the closing of the H_2O window counteracts the growth of λ that would otherwise result from a pure Planck response through a spectral window of fixed width. In fact by $T_\mathrm{s} = 305$ K, the window has nearly closed in our climate model.

Finally, the third category of λ_ν includes the spectral regions within which CO_2 does have appreciable opacity. For low CO_2 concentrations, this occurs only within the 15-μm band centered at 667.5 cm^{-1} (and also around 2300 cm^{-1}, although those higher wavenumbers are not shown in Fig. 2 because the reduced amplitude of the Planck function limits their importance). Because CO_2 is not a condensible gas for Earthlike temperatures, its concentration is well-mixed in the vertical, and its optical depths are *not* invariant functions of temperature within the atmosphere. In fact if one neglects the explicit temperature-scaling of absorption coefficients, CO_2 optical depths are invariant functions of *pressure* rather than temperature. This leads to a decidedly non-Simpsonian spectral feedback behavior in CO_2-influenced portions of the longwave spectrum.

The climate-stabilizing influence of this third spectral category is clear from the $T_\mathrm{s} = 305$ K case depicted in Figure 2. At that surface temperature, were it not for the presence of a significant amount of CO_2 in the atmosphere, the spectral region around 15-μm would behave in the Simpsonian manner, with $\lambda_\nu \simeq 0$, due to the high opacity of H_2O there. But, because CO_2 is well-mixed and therefore does not behave in a Simpsonian manner, λ_ν exhibits prominent peaks on either side of the 15 μm band. (The spectral feedback goes to 0 at the core of the band because its emission levels are well into the isothermal stratosphere.) The evocative term "radiator fin" was introduced by Pierrehumbert (1995) to emphasize the importance of relatively dry regions of the tropics and subtropics within which the OLR is relatively more responsive to surface warming (i.e., the local water-vapor feedback in these regions is suppressed due to the climatologically-low RH). Here we use the term "CO_2 radiator fin" as a spectral analogy to this concept, to emphasize the importance of CO_2-dominated portions of the longwave spectrum in allowing OLR to increase in response to surface warming. As we will see, this behavior becomes especially important in the absence of H_2O windows at high T_s.

To make these categorizations precise, we first smooth the surface optical depth data with a centered mean of window width 25 cm^{-1} (this mean is taken geometrically rather than arithmetically; see the thick lines in Fig. 2). Next, using this spectrally-smoothed optical depth data, we define CO_2 radiator fins as having $\tau_\mathrm{s}^{CO_2} > 0.5$, and define H_2O windows as spectral regions that are not CO_2 radiator fins and for which $\tau_\mathrm{s}^{H_2O} < 3$. Figure 2 shows that decomposing the spectrally-resolved feedbacks according to these definitions matches by eye the different regimes exhibited by λ_ν and how they change with varying CO_2, H_2O, and T_s. With these objective definitions of H_2O windows and CO_2 radiator fins, we can then decompose the total λ at each T_s into the contributions from the three types of spectral regions described above. We will refer to the integral of λ_ν over H_2O windows as λ_{H_2O}, and the integral of λ_ν over CO_2 radiator fins as λ_{CO_2}.

This decomposition is shown in Figure 3. As the surface temperature increases, the H_2O windows close, and λ_{H_2O} heads toward zero. Since λ is dominated by λ_{H_2O} at low CO_2 and T_s, λ also tracks sharply downwards for $T_\mathrm{s} < 305$ K or so. At the same time, the strength of the CO_2 radiator fins increases monotonically with T_s and CO_2, and in

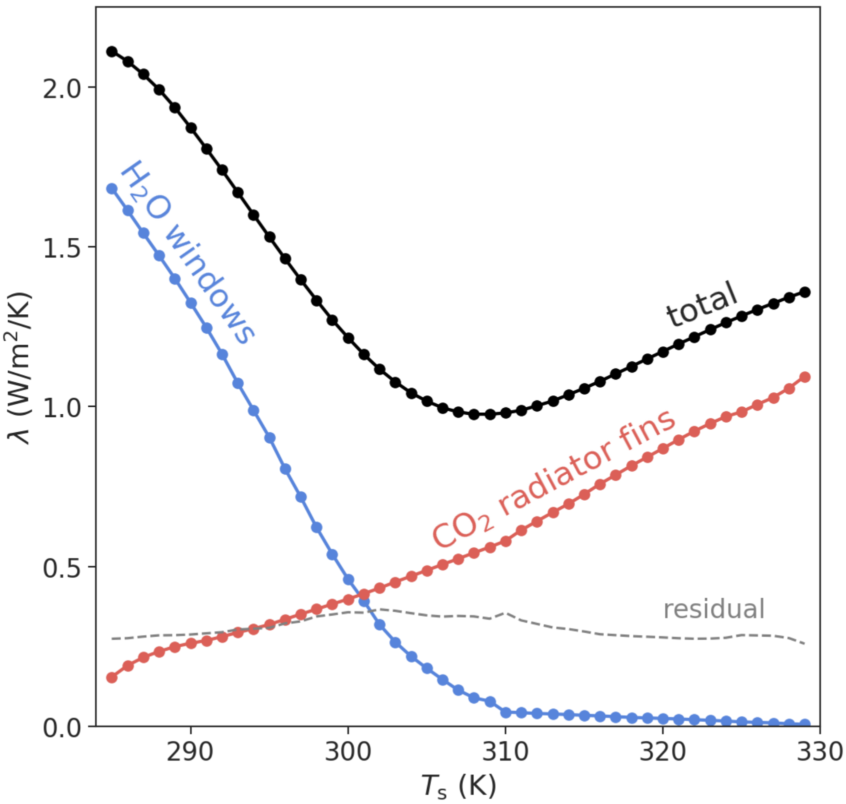

Figure 3. The total differential feedback parameter λ (black), and its decomposition into contributions from H_2O windows (blue) and CO_2 radiator fins (red). At low T_s and CO_2 the feedback is dominated by the H_2O windows, whereas at high T_s and CO_2 the feedback is dominated by the CO_2 radiator fins. See the main text for the definitions of these categories.

fact λ_{CO_2} grows to dominate the total feedback by around $T_s > 310$ K. Spectral regions that do not meet the criteria for H_2O windows or CO_2 radiator fins, which are presumed to behave in an approximately Simpsonian manner, contribute a small positive feedback that is roughly constant with T_s. One gets the impression that the job of climate stabilization is a two-part relay, with the minimum in λ (and the maximum ECS) occurring around the surface temperature at which a nearly exhausted λ_{H_2O} passes the baton on to a λ_{CO_2} that has not yet reached full steam.

The closing of the H_2O windows at high surface temperature is to be expected from the Clausius-Clapeyron scaling of water vapor path (Koll & Cronin, 2018). But what causes the strengthening of the CO_2 radiator fins? In general, the phenomenology of spectral OLR can be understood via the so-called emission-level (EL) approximation, which says that radiative emission to space originates from a suitably chosen emission level with optical depth τ_{em} of $\mathcal{O}(1)$. Within the EL framework, changes in OLR$_\nu$ with T_s (i.e., λ_ν) can then be related to changes in the *emission temperature* T_{em}, which is the temperature at which $\tau = \tau_{\text{em}}$:

$$\lambda_\nu \simeq \pi \frac{dB_\nu}{dT}\bigg|_{T_{\text{em}}} \Delta T_{\text{em}}, \tag{7}$$

where B_ν is the Planck function at wavenumber ν and ΔT_{em} is the change in emission temperature resulting from a 1-K increase in surface temperature (and associated moist-adiabatic warming). The physics of equation (7) is central to our understanding of the

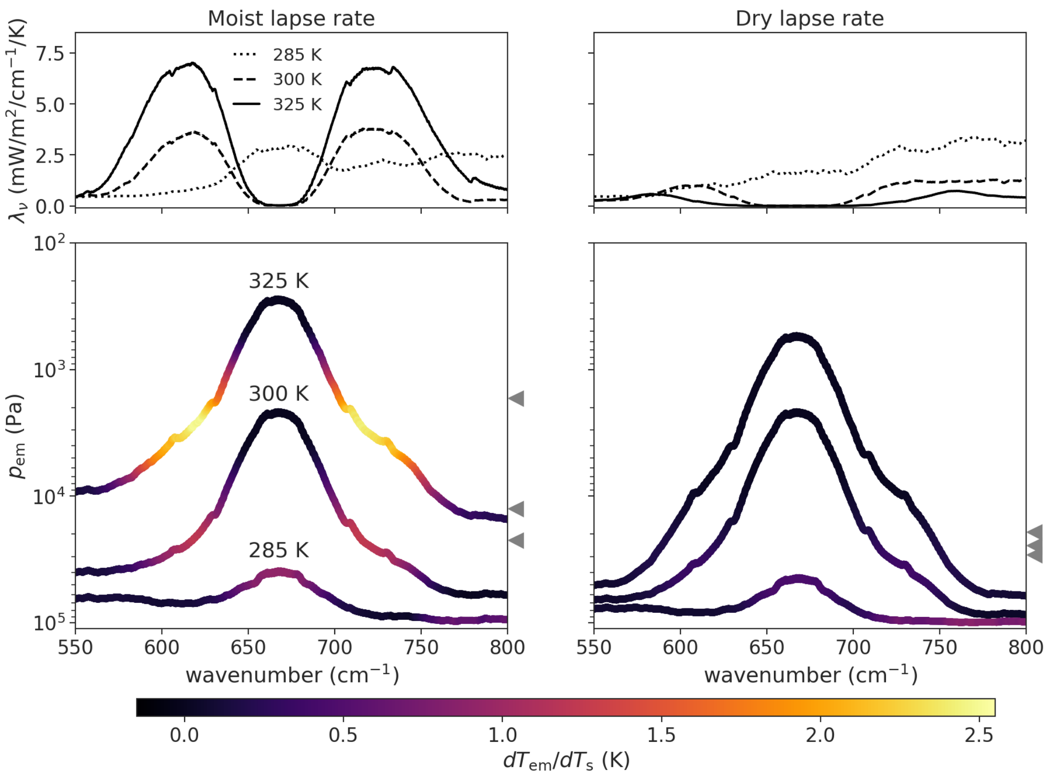

Figure 4. (Top row) Smoothed λ_ν in the vicinity of 15 μm, for T_s = 285, 300, and 325 K. As in Figure 2, the smoothing is performed as a centered mean with window width 25 cm^{-1}. (Bottom row) Smoothed emission pressures (where $\tau = \tau_{em} = 0.56$), color-coded according to the smoothed change in emission temperature. The triangles at the right of the plot mark the tropopause pressures (with high-to-low tropopause pressures corresponding to low-to-high surface temperatures). The left column shows results from the standard configuration of our climate model, with the tropospheric lapse rate set by the moist pseudoadiabat; the right column shows results from a version of the model that assumes a dry-adiabatic troposphere.

Simpsonian spectral intervals which we have already discussed at length: because $\tau \simeq \tau(T)$ for H_2O-dominated wavenumbers, T_{em} becomes approximately fixed once the atmosphere becomes optically thick at such wavenumbers, and $\lambda_\nu \simeq 0$.

In Figure 4, we seek to better understand the strengthening of the CO_2 radiator fins through this EL framework. Focusing on the first column for now (which corresponds to the standard configuration of our climate model), the top row shows the (smoothed) λ_ν in the spectral interval centered around 15 μm for three surface temperatures that span our parameter range (285, 300, and 325 K). The lower row shows the (smoothed) emission pressures (i.e., the pressure at which $\tau = \tau_{em}$) for these same three surface temperatures, color-coded by the (smoothed) change in emission temperature caused by a 1-K increase in surface temperature. We choose to define our emission level as occurring at $\tau_{em} = 0.56$, although our results are largely unchanged as long as τ_{em} is $\mathcal{O}(1)$; see Appendix B of Jeevanjee et al. (2020) for further discussion of the choice in τ_{em}. For each surface temperature, the tropopause pressure is marked by a triangle at the right edge of the plot. The right column of Figure 4 shows the same analysis for a version of our climate model that uses a dry-adiabtic lapse rate in the troposphere instead of a moist pseudoadiabat; we discuss these results in more detail in section 3.3.

At low CO_2 and T_s (i.e., the 285 K case), the emission pressures at the core of the CO_2 band are *below* the tropopause. As a result, when the surface and troposphere are warmed, the emission temperatures increase at the core of the band and λ_ν exhibits a single peak there. However, since the moist pseudoadiabatic lapse rate approaches the dry adiabat at cold surface temperatures, this upper-tropospheric warming is not enhanced relative to the surface warming of 1 K imposed to compute the differential feedback, so ΔT_{em} is not very large.

At higher CO_2 and T_s (i.e., the 300 K case), the emission pressures at the core of the CO_2 band occur well above the tropopause, so it is only on the wings of the CO_2 band that emission levels occur within the troposphere and can respond to the tropospheric warming. At the edges of the CO_2 band, however, where opacity from H_2O starts to dominate over opacity from CO_2, the spectral feedback again approaches zero due to the Simpsonian behavior of H_2O-dominated wavenumbers. This causes λ_ν to exhibit a twin-peaked structure rather than the single peak observed at lower T_s and CO_2. In addition, at the warmer surface temperature of 300 K, the magnitude of the upper-tropospheric warming is notably enhanced compared to the surface warming of 1 K, which increases the amplitude of the twin peaks. These trends are continued for the 325 K case, with the twin-peaked CO_2 radiator fin growing stronger yet as the moist-adiabatic upper-tropospheric warming is further enhanced.

It can be inferred from Figure 4 that the decreasing pressure of emission levels at progressively higher CO_2 and T_s is an important ingredient of the strengthening CO_2 radiator fins. As T_s increases, the ever more amplified warming in the deepening upper troposphere occurs at ever increasing heights. If the emission levels in the CO_2 band did not keep pace with the rapidly deepening troposphere, this amplified upper-tropospheric warming would quickly become inaccessible to the CO_2 radiator fins, and their strength would be diminished because ΔT_{em} would be limited by the smaller warming of the lower troposphere. We will return to this idea in section 3.3, in which we perform mechanism-denial tests.

While moist-adiabatic warming at fixed p sets an upper bound on ΔT_{em}, in reality, two effects with the same sign cause ΔT_{em} to fall well short of the limit set by $dT/dT_s|_p$. These effects are 1) the explicit temperature-dependence of CO_2 absorption coefficients, which is important even when H_2O opacity can be neglected; and 2) overlap with H_2O opacity, which is most important at the edges of the CO_2 band (Figure S2). Unfortunately, these effects are not amenable to a simple analytical treatment, so we are stuck using the output of the RFM to diagnose changes in T_{em}. However, a qualitatively accurate understanding of the behavior of λ_ν within the CO_2 radiator fin is provided by combining enhanced upper-tropospheric warming on a moist adiabat with a progressively deepening CO_2 emission peak.

3.3 Mechanism denial tests

Figure 3 shows that the existence of the minimum in λ, and the resulting peak in ECS, results from the strengthening of the CO_2 radiator fins and the closing of the H_2O windows. To test this conclusion, we performed several mechanism denial tests to prevent various aspects of the relevant physics from playing their role in establishing the λ minimum.

We first repeated our calculations without including the H_2O continuum, in which case the H_2O windows do not close even at the highest surface temperatures we consider, and the total feedback parameter remains large across our parameter range (Fig. 5, left). Next, we modified our climate model to use a dry-adiabatic lapse rate in the troposphere instead of the moist pseudoadiabat. Since warming on a dry-adiabat is not enhanced in the upper troposphere, this change prevents the rapid warming of the CO_2 emission levels at high surface temperature, which is a key ingredient of the strengthening of the CO_2

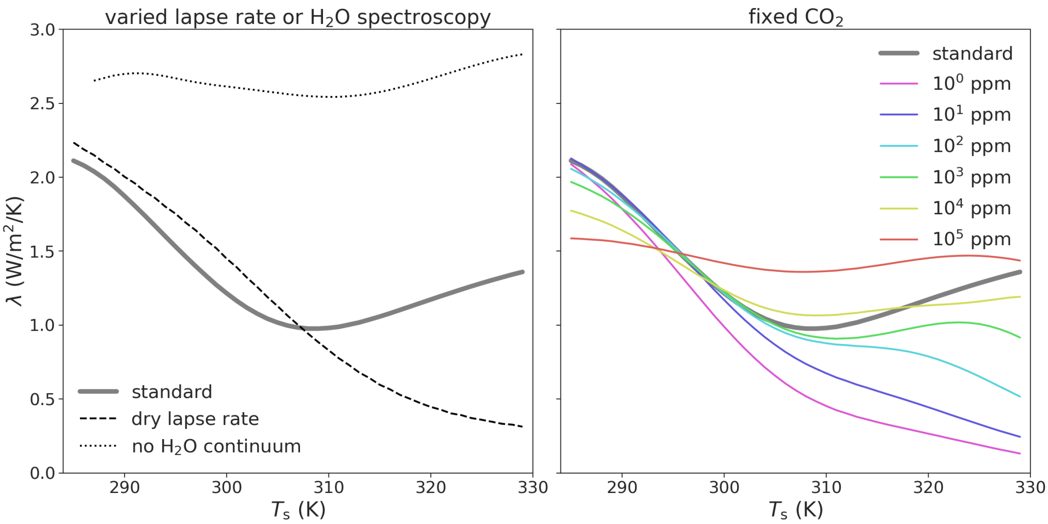

Figure 5. (left) A comparison of the differential feedback parameter λ for the standard configuration of our climate model, a version that assumes a dry-adiabatic troposphere, and a version that neglects H_2O continuum opacity in the radiative transfer calculations. (right) A comparison of λ calculated with varying fixed amounts of CO_2 instead of the energetically-consistent varying amount of CO_2 at each T_s.

radiator fins at high CO_2 and T_s (see also the second column of Fig. 4). As a result, in this case the total feedback parameter tracks the dwindling strength of the H_2O windows, and there is no minumum in λ (Fig. 5, left). This behavior is expected in a traditional "runaway" scenario, where the OLR becomes decoupled from the surface temperature. Therefore, we see that moist convection (i.e., the establishment of a moist-adiabatic troposphere) stabilizes the system against the possibility of a runaway in comparison to a climate system with a dry-adiabatic troposphere.

As can be inferred from Figure 4, the strengthening of the CO_2 radiator fins at high T_s is also dependent on the energetically-consistent increase of CO_2 with T_s. We explore this further in the right panel of Figure 5 by recalculating the differential feedback parameter as a function of T_s but with fixed amounts of CO_2. For small amounts of CO_2 (100 ppm or less), the deepening upper troposphere outgrows the CO_2 emission levels at high T_s, preventing the strengthening of the CO_2 radiator fins. As a result, λ decreases monotonically as a function of T_s for small CO_2 inventories, although the approach to zero (the runaway limit) is delayed by adding more CO_2 (consistent with the analysis of Koll & Cronin (2018)). At higher CO_2 concentrations (1000 ppm or more), there is a very shallow minimum in λ. Even this shallow minimum in λ all but disappears for a constant, very high concentration of CO_2 of 10^5 ppm.

In summary, these mechanism denial tests have shown that the ECS peak in our climate model depends on 1) an H_2O continuum to quickly close the windows; 2) moist-adiabatic tropospheric temperatures to provide enhanced upper-tropospheric warming; and 3) a progressively deepening CO_2 peak to take full advantage of (2).

4 Discussion

We have demonstrated here a longwave, clear-sky mechanism for the ECS peak around $T_s = 310$ K. But, much work remains to be done to establish whether this mechanism governs the ECS peak seen in comprehensive climate models. Shortwave feedbacks, which we have neglected here, are sure to play a role. Models also exhibit a radiative-convective transition around $T_s = 310$ K which changes the structure of the boundary-layer and low clouds (Popp et al., 2016; Wolf & Toon, 2015; Wordsworth & Pierrehumbert, 2013), which could also amplify or modulate the ECS peak studied here. Further work, likely involving mechanism-denial experiments across a model hierarchy (Jeevanjee et al., 2017), will be needed to determine which mechanisms dominate, and whether the ECS peaks seen across models indeed have a common cause.

Even if the longwave clear-sky mechanism discussed here does not dominate in comprehensive models, the results of this paper nonetheless help shed new light on climate feedbacks. For instance, the spectral feedback decomposition shown in Figure 3 yields a new perspective on climate sensitivity, which would be difficult to glean from the more conventional Planck + water vapor + lapse rate decomposition. In particular, the λ_{CO_2} component highlights the climate-stabilizing role of the non-Simpsonian CO_2 "radiator fins", especially in combination with moist-adiabatic upper-tropospheric warming (Fig. 4).

Further study of λ_{CO_2} could also clarify the possibility of CO_2-induced runaway greenhouse states. Previous studies in an astronomical context are often focused on habitability and so do not equilibrate CO_2 concentrations with T_s at a given insolation (Ramirez et al., 2014; Goldblatt et al., 2013; Wordsworth & Pierrehumbert, 2013). For equilibrated, energetically consistent calculations such as ours, however, the results shown here suggest that the *increase* in CO_2 with increasing T_s yields a constantly strengthening CO_2 radiator fin which is able to keep climate stable up to relatively high CO_2 and T_s. Further work could test this idea by pushing CO_2 and T_s to much higher values than those considered here. Such efforts would need to incorporate shortwave radiative transfer, because for very large CO_2 inventories, the enhanced planetary albedo from enhanced Rayleigh scattering would effectively decrease the F_{2x} inferred from longwave-only calculations (Forget et al., 2013). This effect would presumably further stabilize the climate against a CO_2-induced runaway.

Acknowledgments
The source code associated with this work will be made publicly available at the corresponding author's GitHub page.

References

Arrhenius, S. (1896). On the influence of carbonic acid in the air upon the temperature of the ground. *Philosophical Magazine Series 5*, *41*(251), 237–276.

Bloch-Johnson, J., Pierrehumbert, R. T., & Abbot, D. S. (2015). Feedback temperature dependence determines the risk of high warming. *Geophysical Research Letters*, *42*(12), 4973–4980.

Clough, S. A., Iacono, M. J., & Moncet, J.-l. (1992). Line-by-line calculations of atmospheric fluxes and cooling rates: Application to water vapor. *Journal of Geophysical Research*, *97*(D14), 15761.

Cousin, C., Doucen, R. L., Boulet, C., & Henry, a. (1985). Temperature dependence of the absorption in the region beyond the 4.3-microm band head of CO(2) . 2: N(2) and O(2) broadening. *Applied optics*, *24*(22), 3899–3907.

Dudhia, A. (2017). The Reference Forward Model (RFM). *Journal of Quantitative Spectroscopy and Radiative Transfer*, *186*, 243–253.

Forget, F., Wordsworth, R., Millour, E., Madeleine, J. B., Kerber, L., Leconte, J., ... Haberle, R. M. (2013). 3D modelling of the early martian climate under a denser CO 2 atmosphere: Temperatures and CO 2 ice clouds. *Icarus*, *222*(1), 81–99. Retrieved from `http://dx.doi.org/10.1016/j.icarus.2012.10.019` doi: 10.1016/j.icarus.2012.10.019

Goldblatt, C., Robinson, T. D., Zahnle, K. J., & Crisp, D. (2013). Low simulated radiation limit for runaway greenhouse climates. *Nature Geoscience*, *6*(8), 661–667.

Gordon, I., Rothman, L., Hill, C., Kochanov, R., Tan, Y., Bernath, P., ... Zak, E. (2017, dec). The HITRAN2016 molecular spectroscopic database. *Journal of Quantitative Spectroscopy and Radiative Transfer*, *203*, 3–69.

Ingram, W. J. (2010). A very simple model for the water vapour feedback on climate change. *Quarterly Journal of the Royal Meteorological Society*, *136*(646), 30–40.

Jeevanjee, N., Hassanzadeh, P., Hill, S., & Sheshadri, A. (2017, jul). A perspective on climate model hierarchies. *Journal of Advances in Modeling Earth Systems*, *9*(4), 1760–1771.

Jeevanjee, N., Seeley, J. T., Paynter, D. J., & Fueglistaler, S. (2020). An analytical model for CO2 forcing, part II: State-Dependence and Spatial Variations. *Submitted to J Climate*.

Knutti, R., & Rugenstein, M. A. (2015). Feedbacks, climate sensitivity and the limits of linear models. *Philosophical Transactions of the Royal Society A: Mathematical, Physical and Engineering Sciences*, *373*(2054).

Knutti, R., Rugenstein, M. A., & Hegerl, G. C. (2017). Beyond equilibrium climate sensitivity. *Nature Geoscience*, *10*(10), 727–736.

Koll, D. D., & Cronin, T. W. (2018, oct). Earth's outgoing longwave radiation linear due to H2O greenhouse effect. *Proceedings of the National Academy of Sciences of the United States of America*, *115*(41), 10293–10298.

Leconte, J., Forget, F., Charnay, B., Wordsworth, R., & Pottier, A. (2013). Increased insolation threshold for runaway greenhouse processes on Earth-like planets. *Nature*, *504*(7479), 268–71.

Manabe, S., Strickler, R. F., Manabe, S., & Strickler, R. F. (1964). Thermal Equilibrium of the Atmosphere with a Convective Adjustment. *Journal of the Atmospheric Sciences*, *21*(4), 361–385.

Meraner, K., Mauritsen, T., & Voigt, A. (2013, nov). Robust increase in equilibrium climate sensitivity under global warming. *Geophysical Research Letters*, *40*(22), 5944–5948.

Mlawer, E. J., Payne, V. H., Moncet, J.-L., Delamere, J. S., Alvarado, M. J., & Tobin, D. C. (2012). Development and recent evaluation of the MT_CKD model of continuum absorption. *Philosophical Transactions of the Royal Society A: Mathematical, Physical and Engineering Sciences*, *370*(1968), 2520–2556.

Pierrehumbert, R. T. (1995). *Thermostats, Radiator Fins, and the Local Runaway Greenhouse* (Vol. 52) (No. 10).

Popp, M., Schmidt, H., & Marotzke, J. (2016). Transition to a Moist Greenhouse with CO2 and solar forcing. *Nature Communications*, *7*.

Ramirez, R. M., Kopparapu, R. K., Lindner, V., & Kasting, J. F. (2014). Can increased atmospheric CO2 levels trigger a runaway greenhouse? *Astrobiology*, *14*(8), 714–731.

Rohling, E. J., Sluijs, A., Dijkstra, H. A., Köhler, P., Van De Wal, R. S., Von Der Heydt, A. S., ... Zeebe, R. E. (2012). Making sense of palaeoclimate sensitivity. *Nature*, *491*(7426), 683–691.

Romps, D. M. (2020). Climate Sensitivity and the Direct Effect of Carbon Dioxide in a Limited-Area Cloud-Resolving Model. *Journal of Climate*, *33*(9), 3413–3429.

Russell, G. L., Lacis, A. A., Rind, D. H., Colose, C., & Opstbaum, R. F. (2013). Fast atmosphere-ocean model runs with large changes in CO2. *Geophysical Research Letters*, *40*(21), 5787–5792.

Seeley, J. T., Jeevanjee, N., Edman, J. P., & Romps, D. M. (2020). An analytical model for CO2 forcing, part I: Logarithmic scaling. *Submitted to J Climate*, 1–19.

Simpson, G. (1928). Some Studies in Terrestrial Radiation. *Memoirs of the Royal Meteorological Society*, *2*(16), 69–95.

Simpson, G. C. (1928, aug). Further studies in terrestrial radiation. *Monthly*

Weather Review, *56*(8), 322–323.
Wolf, E. T., Haqq-Misra, J., & Toon, O. B. (2018). Evaluating Climate Sensitivity to CO2 Across Earth's History. *Journal of Geophysical Research: Atmospheres*, *123*(21), 11,861–11,874.
Wolf, E. T., & Toon, O. B. (2015). The evolution of habitable climates under the brightening Sun. *Journal of Geophysical Research: Atmospheres*, *120*, 5775–5794.
Wordsworth, R. D., & Pierrehumbert, R. T. (2013). Water loss from terrestrial planets with CO2-rich atmospheres. *Astrophysical Journal*, *778*(2).
Zhong, W., & Haigh, J. D. (2013). The greenhouse effect and carbon dioxide. *Weather*, *68*(4), 100–105.